Inorganic Chemistry

Article

pubs.acs.org/IC

Rapid and Highly Sensitive Dual-Channel Detection of Cyanide by Bis-heteroleptic Ruthenium(II) Complexes

Snehadrinarayan Khatua,[†] Debabrata Samanta,[†] Jan W. Bats,[‡] and Michael Schmittel*[,†]

[†]Center of Micro and Nanochemistry and Engineering, Organische Chemie I, Universität Siegen, Adolf-Reichwein-Strasse 2, D-57068 Siegen, Germany

[‡]Institut für Organische Chemie und Chemische Biologie, Johann Wolfgang Goethe-Universität, Max-von-Laue Strasse 7, D-60438 Frankfurt am Main, Germany

Supporting Information

ABSTRACT: Two new ruthenium complexes $[Ru(bipy)_2(\mathbf{PDA})]^{2+}$ (**1**) and $[Ru(phen)_2(\mathbf{PDA})]^{2+}$ (**2**) (**PDA** = 1,10-phenanthroline-4,7-dicarboxaldehyde) have been synthesized to detect cyanide based on the well-known formation of cyanohydrins. Both $\mathbf{1}[\mathbf{PF_6}]_2$ and $\mathbf{2}[\mathbf{PF_6}]_2$ were fully characterized by various spectroscopic techniques and their solid state structures determined by single-crystal X-ray diffraction. Their anion binding properties in pure and aqueous acetonitrile were thoroughly examined using two different channels, i.e., UV−vis absorption and photoluminescence (PL). After addition of only 2 equiv of CN^-, the PL intensity of $\mathbf{1}[\mathbf{PF_6}]_2$ and $\mathbf{2}[\mathbf{PF_6}]_2$ was enhanced ~55-fold within 15 s along with a diagnostic blue shift of the emission by more than 100 nm. PL titrations of $\mathbf{1}[\mathbf{PF_6}]_2$ and $\mathbf{2}[\mathbf{PF_6}]_2$ with CN^- in CH_3CN furnished the very high overall cyanohydrin formation constants $\log \beta_{[CN^-]} = 15.36 \pm 0.44$ ($\beta_{[CN^-]} = 2.3 \times 10^{15}\ M^{-2}$) and $\log \beta_{[CN^-]} = 16.37 \pm 0.53$ ($\beta_{[CN^-]} = 2.3 \times 10^{16}\ M^{-2}$), respectively. For both probes, the second constant, K_2, is about 57−84 times less than K_1, suggesting that the cyanohydrin reaction is stepwise. The stepwise mechanism is further supported by results of a ^1H NMR titration of $\mathbf{2}[\mathbf{PF_6}]_2$ with CN^-. The high selectivity of $\mathbf{2}[\mathbf{PF_6}]_2$ for CN^- was established by PL in the presence of other competing anions. Furthermore, the color change from orange-red to yellow and the appearance of a orange luminescence, which can be observed by the naked eye, provides a simple real-time method for cyanide detection. Finally, theoretical calculations were carried out to elucidate the details of the electronic structure and transitions involved in the ruthenium probes and their cyanide adducts.

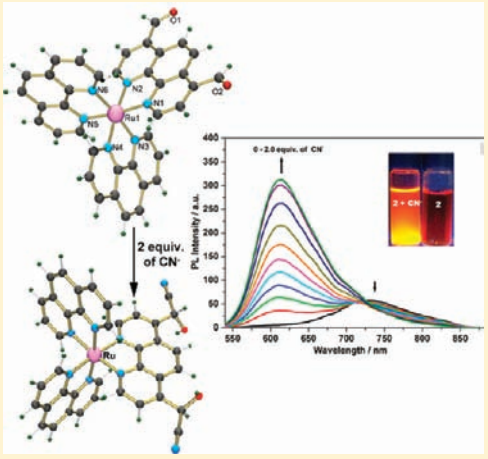

INTRODUCTION

Cyanide as an extremely toxic inorganic anion is harmful to the environment and human health.[1] However, its wide range of application, particularly in gold mining, electroplating, and various chemical industries, leads to unavoidable environmental spills.[2] Due to its serious toxicity and wide use, development of further new probes for highly selective cyanide detection and quantification are desirable.[3] Due to the known limitations of various colorimetric and fluorometric cyanide receptors,[4] such as slow reaction rate,[4a,b] special requirements (e.g., heating),[4c,d] and poor selectivity regarding fluoride or acetate as interfering anions,[4a,b,e,f] reaction-based sensors or chemodosimeters attract great attention.[5] Most chemodosimeters for cyanide so far are based on dyes equipped with a metal binding unit[6] or on covalent bond formation.[7]

Ruthenium(II) polypyridyl complexes of 2,2′-bipyridine (bpy), 1,10-phenanthroline (phen), and related ligands have interesting photophysical, photochemical, and electrochemical properties that make them attractive for development of luminescent sensors,[4b,8] dye-sensitized solar cells (DSSC),[9] photoinduced switches,[10] and photoactive devices.[11] Use of phosphorescent ruthenium(II) polypyridine complexes as chemosensors or probes[12] has recently attracted enormous interest owing to their advantageous photophysical properties, such as visible excitation wavelengths, large Stoke shifts, relatively long excited state lifetimes, suitable redox properties for electrochemiluminescence, and high stability in aqueous media compared with those of pure organic luminophores. In recent years, a large number of chromogenic and luminescent receptors/probes based on ruthenium(II) polypyridine complexes has been developed for the selective and sensitive sensing of metal cations,[13] anions,[14] molecular oxygen,[15] and biologically relevant molecules.[16]

While bisheteroleptic ruthenium complexes have previously been used for both cation and anion detection, only a few are selective and sensitive toward the cyanide ion. In many cases, however, fluoride and acetate were strongly interfering anions.[17] Recently, addition of anions, such as cyanide (CN^-), to an electron-deficient carbonyl unit has been

Received: October 21, 2011
Published: March 14, 2012

   dx.doi.org/10.1021/ic2022853 | *Inorg. Chem.* 2012, 51, 7075−7086

Chart 1. Chemical Structures of the Ligand and Ruthenium Complexes

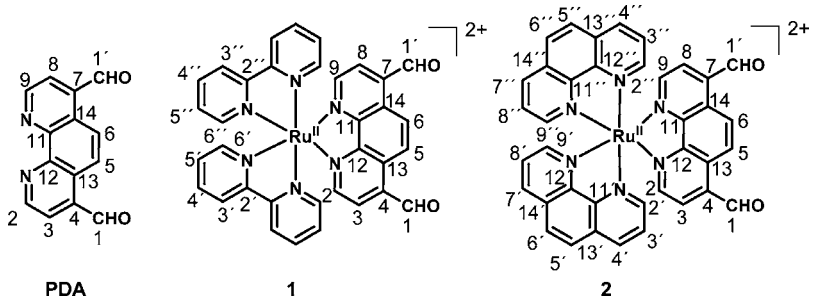

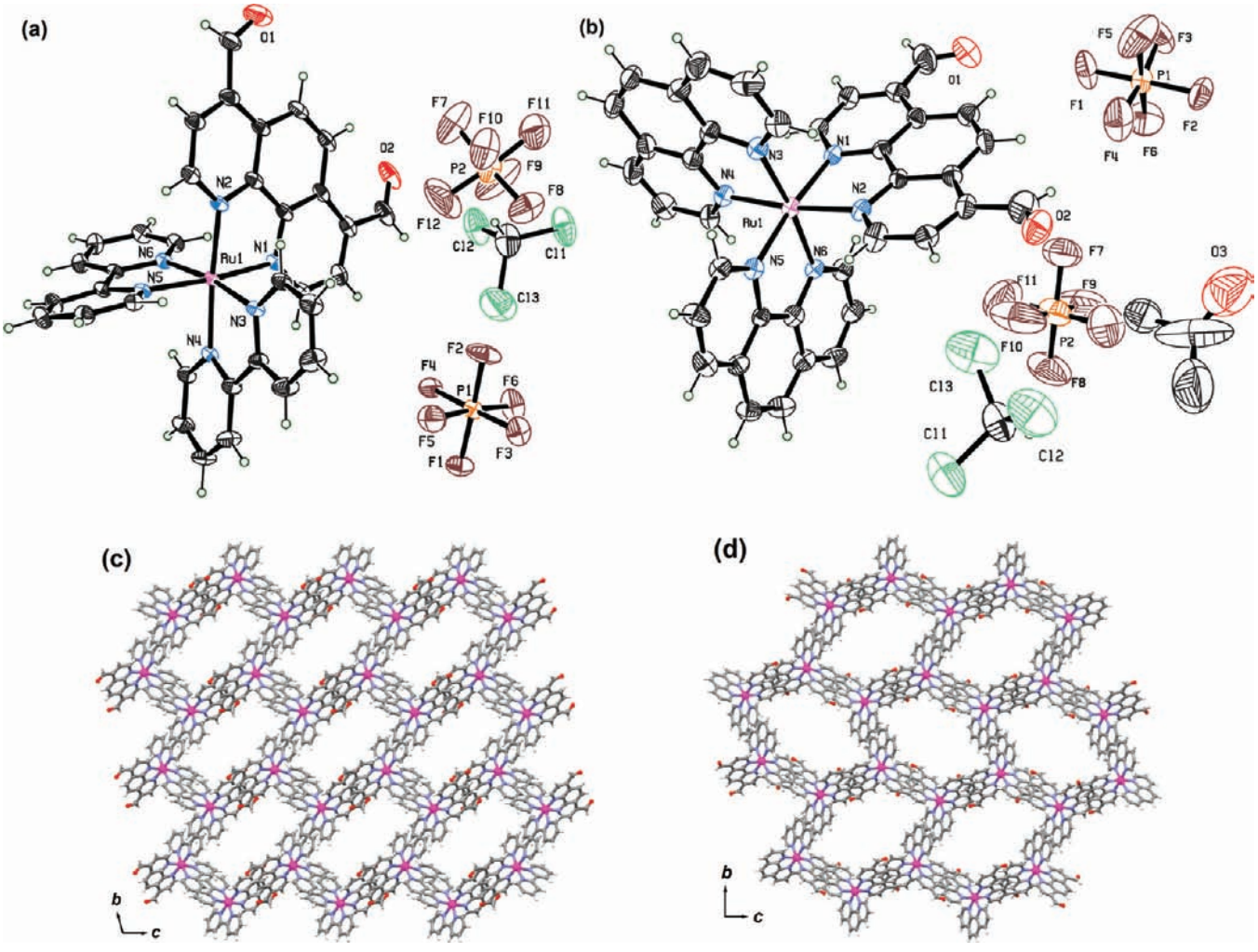

Figure 1. Crystal structure of (a) compound $\mathbf{1}[PF_6]_2$ and (b) compound $\mathbf{2}[PF_6]_2$ (thermal ellipsoids were drawn at the 30% probability level). Only non-carbon and non-hydrogen atoms except fluorine are labeled here. View of the three-dimensional (3-D) crystal packing of (c) compound $\mathbf{1}[PF_6]_2$ and (d) compound $\mathbf{2}[PF_6]_2$ along the crystallographic *a* axis. Solvent molecules and counter PF_6^- ions are omitted for clarity.

successfully applied in the design of colorimetric or turn-on fluorescent probes. Cyanide has a particularly strong affinity to C═O (see its well-known formation of a cyanohydrin),[7a,b,d] and thus, the interference of acetate and fluoride may be reduced successfully.[18] Moreover, to establish higher kinetic reactivity and equilibrium constants, stronger electron-withdrawing groups, such as the $-C(=O)CF_3$ group, are advised.[19] Instead, the electron deficiency of a functional group or the acidity of a specific proton of an organic ligand may be significantly increased when it is coordinated to a positive metal center like Ru^{2+}, Co^{2+}, etc.[20]

As part of our ongoing research in multichannel probes based on ruthenium(II) and iridium(III) diimine complexes,[21] we recently started to evaluate bis-heteroleptic ruthenium(II) complexes as anion probes. Due to the above-mentioned advantages of ruthenium(II) complexes as probes and of the carbonyl group as a selective colorimetric and fluorescent cyanide reaction site, we designed the two ruthenium complexes $[Ru(bipy)_2(\mathbf{PDA})]^{2+}$ (**1**) and $[Ru(phen)_2(\mathbf{PDA})]^{2+}$ (**2**) (**PDA** = 1,10-phenanthroline-4,7-dicarboxaldehyde). In the current work, their synthesis and aptness for luminescence detection of CN^- based on the well-known cyanohydrin

dx.doi.org/10.1021/ic2022853 | *Inorg. Chem.* 2012, 51, 7075–7086

formation at the aldehyde group are presented. As expected, both $\mathbf{1}[PF_6]_2$ and $\mathbf{2}[PF_6]_2$ reacted preferably with cyanide even in the presence of competitive anions, namely, F^-, Cl^-, Br^-, I^-, OAc^-, $H_2PO_4^-$, HSO_3^-. The two aldehyde groups of both complexes reacted with cyanide in a stepwise manner, as disclosed, for example, by ^1H NMR titration. Theoretical calculations were made to assign the electronic transitions in **1** and **2** and their cyanide adducts. The results indicate a partial MLCT switching after reaction with cyanide.

RESULTS AND DISCUSSION

Synthesis and Characterization. The anion-responsive phenanthroline **PDA** was prepared according to a reported but modified procedure.[22] Ruthenium compounds $\mathbf{1}[PF_6]_2$ and $\mathbf{2}[PF_6]_2$ were synthesized by refluxing **PDA** with *cis*-$Ru(bpy)_2Cl_2{\cdot}2H_2O$ and *cis*-$Ru(phen)_2Cl_2$, respectively, in ethanol/water (2:1) under nitrogen followed by anion exchange of Cl^- with PF_6^- (Chart 1). Dark red and black crystals of $\mathbf{1}[PF_6]_2$ and $\mathbf{2}[PF_6]_2$ were obtained from $CH_3COCH_3/CHCl_3/CH_2Cl_2$ (3:2:1) in 63% and 60% yield, respectively. Both $\mathbf{1}[PF_6]_2$ and $\mathbf{2}[PF_6]_2$ were fully characterized by elemental analysis, 1D (^1H, ^{13}C) and 2D NMR ($^1H-^1H$ COSY, $^1H-^{13}C$ HSQC, and $^1H-^{13}C$ HMBC) spectroscopy (Figures S4–S13, Supporting Information), ESI-MS spectrometry (Figure S14 and S15, Supporting Information), electrochemical studies (Figure S16, Supporting Information), and single-crystal X-ray diffraction (Figure 1). Photophysical properties were determined by UV–vis and PL spectroscopy (Figure 2).

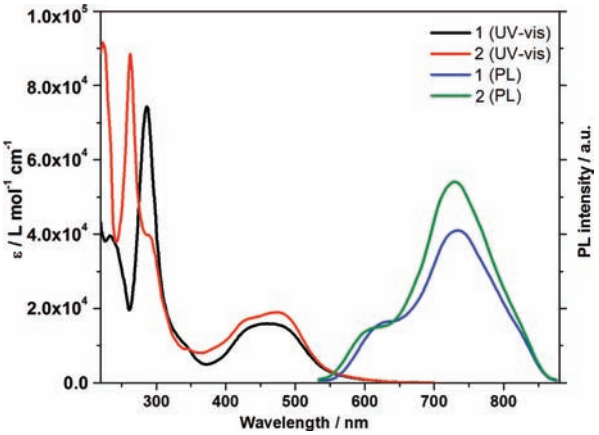

Figure 2. UV–vis (black line, red line) and PL (blue line, green line) spectra of $\mathbf{1}[PF_6]_2$ and $\mathbf{2}[PF_6]_2$, respectively, measured in acetonitrile at room temperature.

The 1D and 2D NMR spectra of $\mathbf{1}[PF_6]_2$ and $\mathbf{2}[PF_6]_2$, recorded in acetone-d_6 at room temperature, clearly show all expected resonances for the phenanthroline and bipyridine ligands. In the ^{13}C spectra of $\mathbf{1}[PF_6]_2$ and $\mathbf{2}[PF_6]_2$ all peaks are fully assigned with the help of HSQC and HMBC. For $\mathbf{1}[PF_6]_2$, the ESI-MS clearly shows two peaks at m/z = 794.6 (calcd 794.6) and 324.8 (calcd. 324.8) that are assigned to $\mathbf{1}{\cdot}(PF_6)^+$ and $\mathbf{1}^{2+}$, respectively. Similarly for $\mathbf{2}[PF_6]_2$, peaks are observed at m/z = 842.1 (calcd 842.7) and 348.3 (calcd 348.3). For both compounds, the experimental isotopic distribution of the singly and doubly charged species is well matching with the calculated one (Figures S14 and S15, Supporting Information). The electrochemical properties of $\mathbf{1}[PF_6]_2$ and $\mathbf{2}[PF_6]_2$ were examined by cyclic voltammetry (CV) using a Pt working electrode in dry CH_3CN under N_2 atmosphere with 1,1′-dimethylferrocene as internal standard ($E_{1/2}{}^{ox}$ = −0.09 V vs $FeCp_2{}^{0/+}$). Compound $\mathbf{1}[PF_6]_2$ shows a quasi-reversible (ΔE_p = 72 mV) Ru^{2+}/Ru^{3+} redox couple at $E_{1/2}{}^{ox}$ = +1.038 V vs $FeCp_2{}^{0/+}$ (Figure S16, Supporting Information). The 128 mV anodic shift in comparison to $[Ru(bipy)_3]^{2+}$ ($E_{1/2}$ = +0.91 V vs $FeCp_2{}^{0/+}$)[23] is readily explained by the stronger π-acceptor quality of ligand **PDA**, effectively decreasing the HOMO energy level. Similarly, for $\mathbf{2}[PF_6]_2$ a quasi-reversible redox wave at $E_{1/2}{}^{ox}$ = +1.04 V vs $FeCp_2{}^{0/+}$ for Ru^{2+}/Ru^{3+} is observed with a peak to peak separation (ΔE_p) of 74 mV. The redox wave is anodically shifted by only 30 mV in comparison to $[Ru(phen)_3]^{2+}$ ($E_{1/2}$ = +1.01 V vs $FeCp_2{}^{0/+}$). The two **PDA**-centered (LC) reduction potentials $E_{1/2}{}^{red}$ for $\mathbf{1}[PF_6]_2$ and $\mathbf{2}[PF_6]_2$ were found at −1.10/−1.43 and −1.05/−1.36 V vs $FeCp_2{}^{0/+}$, respectively. In contrast, the reduction waves for the bipy ligands ($E_{1/2}{}^{red}$ = −1.89/−2.08, −2.28 V vs $FeCp_2{}^{0/+}$) and phen ligands ($E_{1/2}{}^{red}$ = −1.81 V and E_{pc} = −2.03 V vs $FeCp_2{}^{0/+}$) were observed at more negative potential (see Figure S16, Supporting Information).

Crystal Structures. Compounds $\mathbf{1}[PF_6]_2$ and $\mathbf{2}[PF_6]_2$ were found to crystallize in the triclinic and monoclinic space group $P\bar{1}$ and $P2_1/n$, respectively. Their structures reveal that both ruthenium centers adopt a similar octahedral geometry through tridentate coordination of two ancillary bipyridines/phenanthrolines and one **PDA** ligand (Figure 1a and 1b). The Ru–N bond distances in $\mathbf{1}[PF_6]_2$ and $\mathbf{2}[PF_6]_2$ are in the range of 2.043(6)–2.070(5) Å, with trans N–Ru–N angles in the range of 170.80(17)–175.84(18)°. Similar bond lengths and angles were also observed in formerly reported ruthenium polypyridyl complexes.[24] Analysis of the crystal packing in both $\mathbf{1}[PF_6]_2$ and $\mathbf{2}[PF_6]_2$ reveals that the complexes form noncovalent 3D networks (Figure 1c and 1d) which are held together by weak C–H···O and C–H···F hydrogen bonds as well as by $\pi-\pi$ stacking interactions of two bipyridines/phenanthrolines of neighboring complexes. The occurrence of C–H···F hydrogen bonds indicates that the counteranion PF_6^- plays an important role in formation of the 3D networks.

Photophysical Properties. UV–vis spectra of $\mathbf{1}[PF_6]_2$ and $\mathbf{2}[PF_6]_2$ in CH_3CN display sharp bands at 287 ($\varepsilon = 7.4 \times 10^4$) and 264 nm ($\varepsilon = 8.8 \times 10^4$), respectively, assigned to intraligand (IL) $\pi-\pi^*$ transitions. Additionally, in both spectra a broad metal-to-ligand charge-transfer (MLCT) absorption is observed in the 370–600 nm range consisting of two or more MLCT bands. For $\mathbf{2}[PF_6]_2$, a band at λ_{max} = 473 nm ($\varepsilon = 1.9 \times 10^4$) and a shoulder at 435 nm ($\varepsilon = 1.7 \times 10^4$) are observed, whereas for $\mathbf{1}[PF_6]_2$ it is impossible to provide an exact absorption maximum due to excessive broadening (Figure 2). Deconvolution of the broad absorption spanning from 370 to 600 nm furnishes two bands at λ_{max} = 472 ($\varepsilon = 1.5 \times 10^4$) and 435 nm ($\varepsilon = 1.4 \times 10^4$). A time-dependent DFT (TD-DFT) calculation was performed to assign those bands (vide infra). Compounds $\mathbf{1}[PF_6]_2$ and $\mathbf{2}[PF_6]_2$ show a rather poor emission intensity at 732 nm upon excitation at 473 and 472 nm, respectively. It is noteworthy that the PL maxima and shapes are independent of the wavelength of excitation (from 400 to 473 nm), which implies that the emission occurs from the same MLCT excited state.

Anion Detection in UV–Vis and Photoluminescence (PL) Channels. The aptitude of $\mathbf{1}[PF_6]_2$ and $\mathbf{2}[PF_6]_2$ to serve as probes for different anions (2.0 equiv) was tested by UV–vis and PL spectroscopy in CH_3CN at room temperature. Both $\mathbf{1}[PF_6]_2$ and $\mathbf{2}[PF_6]_2$ gave a similar response to anions and

dx.doi.org/10.1021/ic2022853 | Inorg. Chem. 2012, 51, 7075–7086

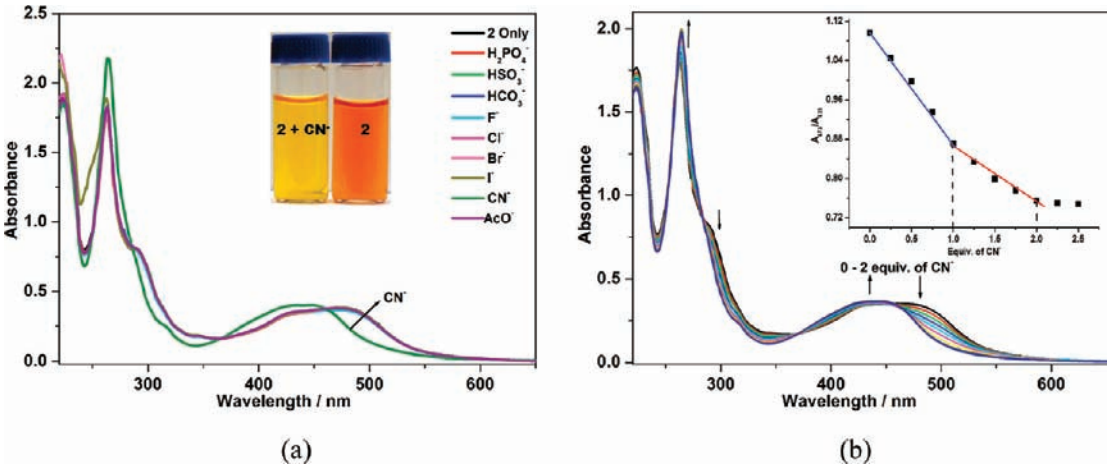

Figure 3. (a) UV−vis absorption spectra of $\mathbf{2}[\mathbf{PF_6}]_2$ (20 μM) with different anions (2.0 equiv). (Inset) Photograph showing the color change from orange red to yellow upon addition of CN^-. (b) UV−vis absorption titration of $\mathbf{2}[\mathbf{PF_6}]_2$ (20 μM) with CN^- solution (0−2.0 equiv) in CH_3CN at 25 °C. (Inset) Plot of A_{473}/A_{435} (ratio of absorbance at 473 and 435 nm) against the amount of added CN^- (lines serve to illustrate the change in stoichiometry).

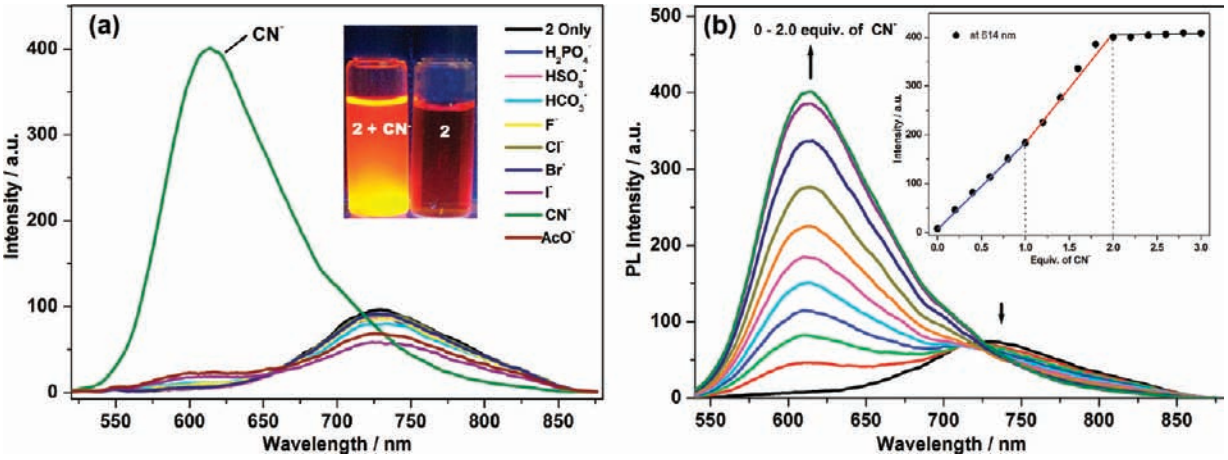

Figure 4. (a) PL spectra of $\mathbf{2}[\mathbf{PF_6}]_2$ (20 μM) with different anions (2.0 equiv). (Inset) Photograph showing the orange luminescence upon addition of CN^-. (b) PL titration of $\mathbf{2}[\mathbf{PF_6}]_2$ (20 μM) with CN^- solution (0−2.0 equiv) in CH_3CN at 25 °C. (Inset) Plot of the PL intensity change ($I - I_0$) at 614 nm upon addition of CN^- (lines serve to illustrate the change in stoichiometry).

equally similar UV−vis and PL titration profiles with specific anions. For brevity, the present discussion will be mostly confined to compound $\mathbf{2}[\mathbf{PF_6}]_2$ (see Supporting Information for corresponding data of compound $\mathbf{1}[\mathbf{PF_6}]_2$). In the UV−vis channel, $\mathbf{2}[\mathbf{PF_6}]_2$ shows notable absorption changes only with CN^-. Significant blue shifts of λ_{max} of $\mathbf{2}[\mathbf{PF_6}]_2$ ($\Delta\lambda$ = 23−38 nm) and the prominent orange-red to yellow color change can be readily observed by the naked eye upon addition of 2.0 equiv of cyanide (Figure 3a, inset). In contrast, no significant changes of λ_{max} and the color were observed in the presence of other anions, such as F^-, Cl^-, Br^-, I^-, AcO^-, HCO_3^-, $H_2PO_4^-$, and HSO_3^- (Figure 3a). This points to a selective reaction of CN^- with the −CHO groups of $\mathbf{2}[\mathbf{PF_6}]_2$, which was furthermore monitored by UV−vis titration to understand the cause of the color change. Addition of increasing amounts of CN^- (0−2.0 equiv) to the CH_3CN solution of $\mathbf{2}[\mathbf{PF_6}]_2$ (20 μM) at room temperature reveals a gradual decrease of the absorbance at 473 nm and appearance of two bands at 435 ($\varepsilon = 1.9 \times 10^4$) and 447 nm ($\varepsilon = 1.8 \times 10^4$) (obtained by deconvolution). No further change is observed after addition of more than 2.0 equiv of CN^- ions (Figure 3b). During the course of the UV−vis titration two isosbestic points were clearly observed in the MLCT region. A first isosbestic point was observed at ∼455 nm during addition of 0−1 equiv of CN^- and a second one at 469 nm when more than 1.0 equiv of CN^- was added (Figure S17a, Supporting Information). A plot of the absorbance ratio at 473 and 435 nm (A_{473}/A_{435}) as a function of the amount of cyanide clearly shows that A_{473}/A_{435} decreases linearly up to 1.0 equiv of CN^- and then with a different slope again from 1.0 to 2.0 equiv of cyanide. Thereafter, the ratio becomes constant, clearly indicating a 1:2 binding stoichiometry of $\mathbf{2}[\mathbf{PF_6}]_2$ and CN^-. The observed relationship should allow for a quantitative determination of cyanide in the UV−vis channel. Similarly for $\mathbf{1}[\mathbf{PF_6}]_2$, the broad MLCT band is blue shifted to 435 and 450 nm (obtained by deconvolution) after 2.0 equiv of CN^- addition (Figure S18 in Supporting Information).

For both $\mathbf{1}[\mathbf{PF_6}]_2$ and $\mathbf{2}[\mathbf{PF_6}]_2$ it is expected that the lower energy MLCT band at ∼473 nm is due to a metal (d orbital) to **PDA** ligand (π^* orbital) charge transfer since the electron-withdrawing character of the two CHO groups and their π conjugation with the phenanthroline should efficiently decrease the LUMO energy. On the other hand, the higher energy band at ∼434 nm is attributed to a metal (d orbital) to ancillary

dx.doi.org/10.1021/ic2022853 | Inorg. Chem. 2012, 51, 7075−7086

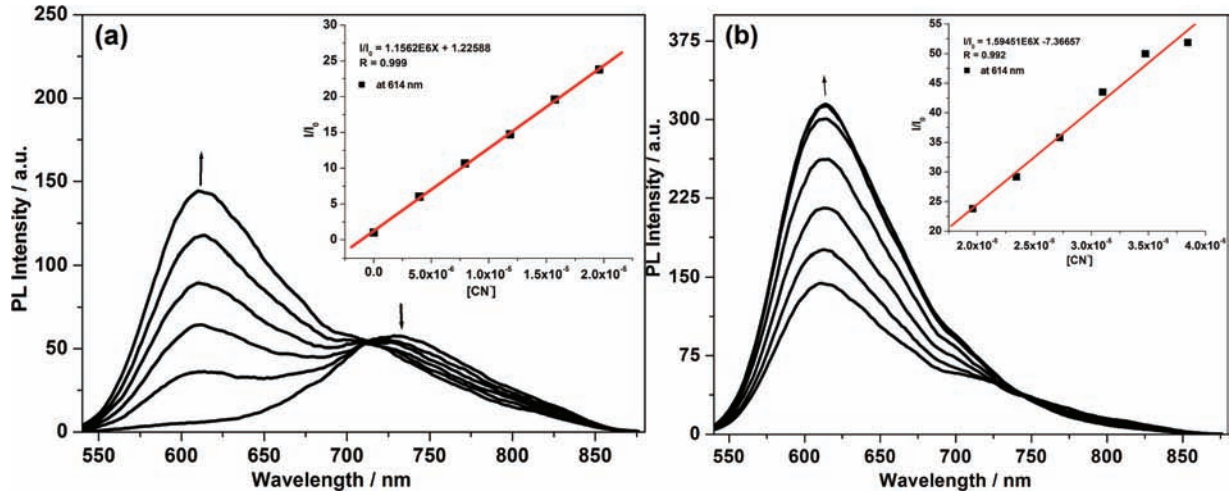

Figure 5. PL titration of $2[PF_6]_2$ adding incremental amounts of CN^-: (a) 0−1.0 and (b) 1.0−2.0 equiv. (Insets) Plot of I/I_0 vs $[CN^-]$ shows a good linear relationship from 0 to 1.0 and 1.0 to 2.0 equiv.

bipy/phen ligand (π^* orbital) charge transfer. A significant enhancement of the LUMO energy level is expected after cyanide addition to the −CHO group due to the much less electron-withdrawing character of the cyanohydrin groups and concomitant loss of extended π conjugation. Hence, after reaction with cyanide, partial or full MLCT switching from ruthenium(II) → **PDA** to ruthenium(II) → bipy/phen(π^*) is expected. To get more details of the changes in the transition, time-dependent DFT (TD-DFT) calculations were performed showing indeed partial MLCT switching from ruthenium(II) → **PDA** to Ru(II) → bipy/phen(π^*) (vide infra).

As stated earlier, compound $2[PF_6]_2$ shows a rather weak emission at 732 nm. Treatment of $2[PF_6]_2$ with 2.0 equiv of various anions shows a notable behavior only with CN^- resulting in a ∼118 nm blue shift of the emission maximum (Figure 4a). The CN^- detection ability of $2[PF_6]_2$ was interrogated through PL titration studies in detail. The titration of $2[PF_6]_2$ (λ_{exc} = 455 nm; isosbestic point of UV−vis titration) shows the gradual disappearance of the PL band at 732 nm with increasing amounts of CN^- ion and the appearance of the new band at 614 nm. No more changes are observed after addition of more than 2.0 equiv of CN^- (Figure 4b). The PL intensity is enhanced ∼52.5-fold (at 614 nm) after addition of 2.0 equiv of CN^-. Similarly for $1[PF_6]_2$, the PL intensity is enhanced ∼55-fold at 624 nm along with a ∼108 nm blue shift after addition of 2.0 equiv of CN^- (Figure S19, in Supporting Information). The cyanohydrin formation constants for CN^- to **1** and **2** were calculated from PL titration data using SPECFIT,[25] which provided $K_1 = 3.6 \pm 2.5 \times 10^8$ M^{-1} ($\log K_1 = 8.56 \pm 0.37$) and $K_2 = 6.3 \pm 1.0 \times 10^6$ M^{-1} ($\log \beta = 15.36 \pm 0.44$; $\beta = 2.3 \times 10^{15}$ M^{-2}) for **1** (average of three individual titrations) and $K_1 = 1.4 \pm 1.2 \times 10^9$ M^{-1} ($\log K_1 = 9.14 \pm 0.46$) and $K_2 = 1.7 \pm 0.3 \times 10^7$ M^{-1} ($\log \beta = 16.37 \pm 0.53$; $\beta = 2.3 \times 10^{16}$ M^{-2}) for **2** (average of three individual titrations).

It is instructive to compare the above data with results from the absorption titrations; for **1** we obtain $\log K = 6.91 \pm 0.10$, $\log \beta = 13.43 \pm 0.18$ and for **2** $\log K = 7.98 \pm 0.14$, $\log \beta = 14.37 \pm 0.24$. Notably, the constants from the absorption measurements are significantly lower than those obtained from PL by 1−2 orders of magnitude. This difference is readily rationalized: In the photoexcited complexes $1[PF_6]_2$ and $2[PF_6]_2$, the MLCT state involves a partial weakening of the π(C═O) bond due to the negative charge in PDA ligand. As a consequence, reaction with cyanide becomes more exothermic, as not a full π(C═O) bond has to be cleaved on the way to the cyanohydrin. The very high overall bond formation constants are in line with CN^- detection through creation of a dynamic covalent bond.

The **PDA** ligand contains not only one but two reactive −CHO groups. As reported earlier for a similar organic probe,[26] cyanide may react with both groups at the same rate. On the other hand, the possibility of a stepwise reaction cannot be ignored. During the PL titration of $2[PF_6]_2$ at first a clear isoemissive point was found at 712 nm up to 1.0 equiv of added CN^-, while a second isoemissive point emerged red shifted to 745 nm upon addition of further CN^-. This suggests the existence of two different equilibria during the course of the titration (Figure 5a and 5b), as equally suggested by the dual-slope relationship (Figure 3b) and two isosbestic points at 455 and 469 nm (Figure S17, Supporting Information) in the UV−vis absorption titration. It is thus reasonable to assume that the two cyanohydrin units are formed in two steps during the titration: first one −CHO group in the complex is attacked by CN^- to form the monocyanohydrin, i.e., 1:1 adduct, then the remaining −CHO group of the 1:1 adduct is attacked by CN^- to yield the 1:2 adduct. As stated earlier, for both **1** and **2** the second binding constant K_2 is approximately 57/84 times smaller than K_1, in full agreement with a stepwise CN^- addition.

When the PL intensity of $2[PF_6]_2$ at 614 nm is plotted against the amount of added CN^-, the graph shows two linear relationsships with different slope, again as in the UV−vis titration; the first one is from 0 to 1.0 equiv of CN^- and the second from 1.0 to 2.0 equiv of CN^-. No more intensity change is observed after more than 2.0 equiv of CN^- has been added, confirming formation of 1:2 adduct, $[\mathbf{2}\text{-}(CN)_2]^{2+}$. (Figure 4b, inset). The plot of the PL intensity change ($I - I_0$) at 614 nm for $2[PF_6]_2$ as a function of the cyanide concentration shows a good linear relationship in the range of 0−1 equiv of cyanide; this indicates that $2[PF_6]_2$ could be used to quantitatively detect the CN^- concentration in an unknown sample (Figure 5, insets).

Selectivity and Sensitivity. To confirm the high selectivity of $2[PF_6]_2$ toward cyanide a competition study was performed. As displayed in Figure 6, no remarkable PL intensity

dx.doi.org/10.1021/ic2022853 | Inorg. Chem. 2012, 51, 7075−7086

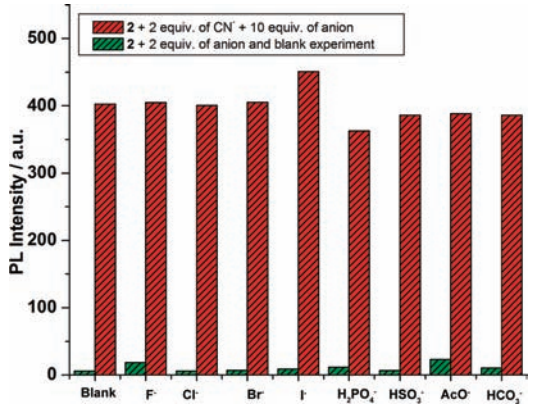

Figure 6. Behavior of $\mathbf{2}[PF_6]_2$ toward CN^- and other anions as measured by PL in CH_3CN.

enhancement was observed upon addition of other possibly competing anions (F^-, Cl^-, Br^-, I^-, $H_2PO_4^-$, HSO_3^-, OAc^-, HCO_3^-; all added in 2 equiv) to the solution of $\mathbf{2}[PF_6]_2$ in CH_3CN in the absence of cyanide. Reversely, addition of 2.0 equiv of CN^- to $\mathbf{2}[PF_6]_2$ in the presence of an excess of other anions (10 equiv) entails a PL enhancement that was well reproducible. Therefore, $\mathbf{2}[PF_6]_2$ may be considered as a highly selective probe for CN^-.

Moreover, $\mathbf{2}[PF_6]_2$ shows a high sensitivity toward CN^- due to the large PL increase, suggesting one to determine the detection limit (DL) for cyanide. For $\mathbf{2}[PF_6]_2$, the PL intensity changes ($I - I_0$) with increasing amounts of cyanide yielded a detection limit as low as ca. 0.18 μM in CH_3CN (Figure S20, Supporting Information). The time course of the PL response of $\mathbf{1}[PF_6]_2$ and $\mathbf{2}[PF_6]_2$ upon addition of 2.0 equiv of cyanide in CH_3CN at room temperature was monitored (Figure 7),

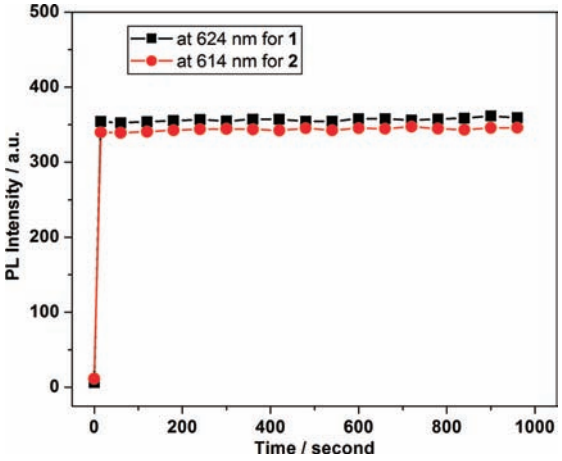

Figure 7. Time course of the photoluminescence response of $\mathbf{1}[PF_6]_2$ and $\mathbf{2}[PF_6]_2$ upon addition of 2.0 equiv of cyanide in CH_3CN at 25 °C.

showing that the maximum of PL for both $\mathbf{1}[PF_6]_2$ and $\mathbf{2}[PF_6]_2$ was reached within 15 s. No further changes were observed from 1 to 15 min. This observation points to an extremely fast reaction of $\mathbf{1}[PF_6]_2$ and $\mathbf{2}[PF_6]_2$ with cyanide. Very recently, Lin et al.[27] also reported on a highly reactive CN^- probe that showed its maximum fluorescence response in less than 1 min but required 5 equiv of CN^- instead of stoichiometric amounts (1 equiv) to complete the reaction. In contrast, probe $\mathbf{2}[PF_6]_2$ shows a higher reactivity as measured by its full response within 15 s, necessitating only the stoichiometric amount (2 equiv) for complete reaction.

Reaction with Cyanide Studied by ^{1}H NMR Spectroscopy and ESI Mass Spectrometry. To obtain further insight into the nature of the reaction of cyanide with $\mathbf{2}[PF_6]_2$, ^{1}H NMR titration was carried out. The incremental addition of tetra-*n*-butylammonium cyanide (TBACN) to a solution of $\mathbf{2}[PF_6]_2$ (2.38 mM) in CD_3CN resulted in incremental upfield shifts of all aromatic proton signals (Figure 8). The spectral shifts practically stop after addition of 2.0 equiv of cyanide. To explain the distinctive changes of the ^{1}H NMR signals during the titration process, we propose formation of two cyanohydrins functions in the 4,7 positions of **PDA** (Scheme 1). During the ^{1}H NMR titration of $\mathbf{2}[PF_6]_2$ with 0–1.0 equiv of CN^- the intensity of the sharp singlet at δ = 10.58 ppm corresponding to the aldehyde protons (1-H, 1′-H) slowly decreases with CN^- concentration and a new peak for the cyanohydrin proton, $-CH(CN)OH$ (1a-H) appears at δ = 4.53 ppm. At the same time, a new signal typical for an aldehyde proton (1″-H) shows up at δ = 10.57 ppm. Simultaneous appearance of the cyanohydrin (1a-H) and a new aldehyde proton (1″-H) clearly indicates that the complex loses its symmetry by forming a 1:1 adduct. The initial signal of the 5,6 protons (5-H, 6-H) of the **PDA** ligand in **2** at δ = 9.36 ppm gradually disappears, and new signals for the 5,6 protons (5a-H, 6a-H) emerge as doublets at δ = 9.13 (d, ^3J = 9.5 Hz, 1H) and 9.28 ppm (d, ^3J = 9.5 Hz, 1H).

Nonequivalence of the 5-H, 6-H protons during titration confirms formation of a 1:1 adduct as well as the stepwise reaction. In complex **2**, the 2-H, 9-H and 3-H, 8-H protons appear as sharp doublets at 8.41 and 8.06 ppm. During titration with up to 1.0 equiv of cyanide, the two doublets shift upfield and separate into two sets due to the unsymmetry of the 1:1 adduct. In the later stage of the titration from 1.0 to 2.0 equiv of CN^- all signals for the 1:1 adduct in **PDA** slowly disappear, except that for the cyanohydrins protons $-CH(CN)$-OH (1a-H).

After addition of 2.0 equiv of CN^-, upfield shifts are observed for the **PDA** ligand ring protons. The signals for 5-H, 6-H at 9.36 ppm, 2-H, 9-H at 8.42 ppm, and 3-H, 8-H at 8.01 ppm were upfield shifted to ~8.85 (for 5b-H, 6b-H), 8.07 (for 2b-H, 9b-H), and 7.68 ppm (for 3b-H, 8b-H), respectively. On the other hand, the signals for the ancillary phenanthroline ligands in **2** remain almost unchanged. The new set of signals, the disappearance of −CHO (1-H, 1′-H), and appearance of new cyanohydrins protons strongly imply formation of the 1:2 adduct, $[\mathbf{2}\text{-}(CN)_2]^{2+}$. It is noted that the 1:2 adduct forms parallel in small amounts at the same time the 1:1 adduct is generated. During the PL titration (vide supra) the two different isoemissive points clearly point to two different equilibria and a stepwise cyanide addition. Thus, ^{1}H NMR titration data strongly support our assumption of a stepwise cyanide addition.

Formation of a 1:2 adduct was further confirmed by ESI-MS. Addition of a slight excess of TBACN to $\mathbf{2}[PF_6]_2$ in CH_3CN revealed a singly positive ion peak at m/z 777.8 that is identified as 1:2 adduct with a cyanide counterion, $[\{\mathbf{2}\text{-}(CN)_2\}^{2+}\cdot(CN)^-]^+$ (calcd 777.7; found, 777.8) (Figure S21, Supporting Information).

Detection of CN^- in Aqueous Solution. For practical use of probe $\mathbf{2}[PF_6]_2$, finally PL titrations were carried out in aqueous solution. As before in acetonitrile, $\mathbf{2}[PF_6]_2$ is weakly emissive at 606 nm in CH_3CN/H_2O (95:5 v/v) upon

dx.doi.org/10.1021/ic2022853 | Inorg. Chem. 2012, 51, 7075–7086

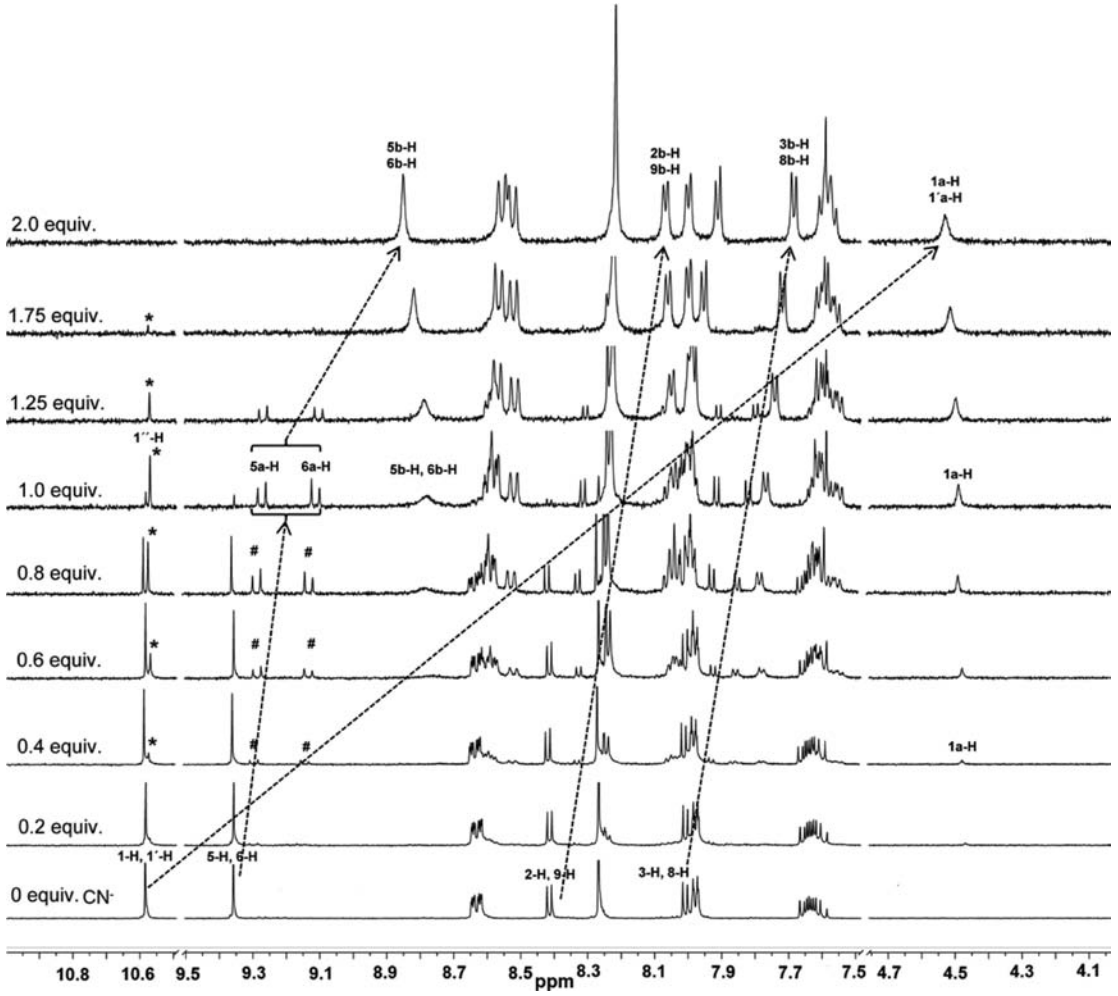

Figure 8. Partial ^{1}H NMR spectra showing the titration of $\mathbf{2}[PF_6]_2$ with CN^- in CD_3CN at room temperature. The asterisks (*) and number (#) signs are used to index specific proton signals of the intermediate 1:1 adduct.

Scheme 1. Cyanide Detection by Probe $\mathbf{2}[PF_6]_2$ Based on Cyanohydrins Formation

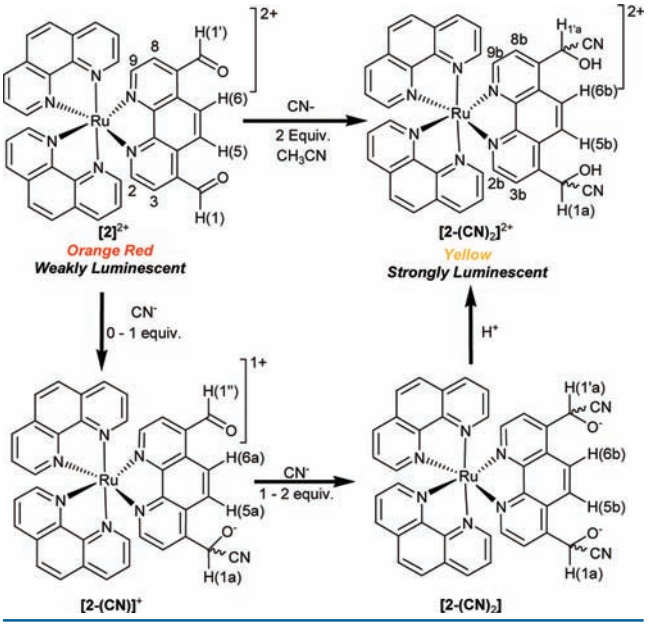

excitation at 455 nm (isosbestic point of the UV–vis titration), and a PL titration with increasing amounts of CN^- shows a gradual enhancement of the intensity at 606 nm. However, unlike the titration process in CH_3CN, here ~5.0 equiv of CN^- is needed to complete the reaction. A study of the time dependence shows that the PL intensity continuously increases up to 15 min, implying a much slower reaction than in pure CH_3CN, where the reaction was completed within 15 s (Figure S22, Supporting Information). This result is consistent with previously reported CN^- probes, where the strong hydration of CN^- in aqueous solution reduces its nucleophilicity.[18c] To set up a test for aqueous solutions, the CN^- reaction was also checked in acetonitrile with lower water content. In 3% aqueous solution (CH_3CN:H_2O; 97:3 v/v), the reaction requires ~3 min to reach the final value, and for completion ~2.5 equiv of CN^- is required. In 1% aqueous solution (CH_3CN:H_2O; 99:1 v/v), CN^- shows a very high reactivity toward $\mathbf{2}[PF_6]_2$ that is almost identical to that in pure CH_3CN (Figure S22, Supporting Information). Using such conditions, i.e., CH_3CN:H_2O = 99:1 (v/v), $\mathbf{2}[PF_6]_2$ is well suited to selectively detect CN^- in aqueous solution and shows equally a good selectivity in competition tests (Figure 9). Actually, $\mathbf{2}[PF_6]_2$ is even slightly more selective and sensitive in acetonitrile after mixing in 1% of water than in the pure organic solvent itself and may be thus of use in real-world applications.

Computational Study. Computational studies were carried out to gain further understanding of the photophysical

dx.doi.org/10.1021/ic2022853 | Inorg. Chem. 2012, 51, 7075–7086

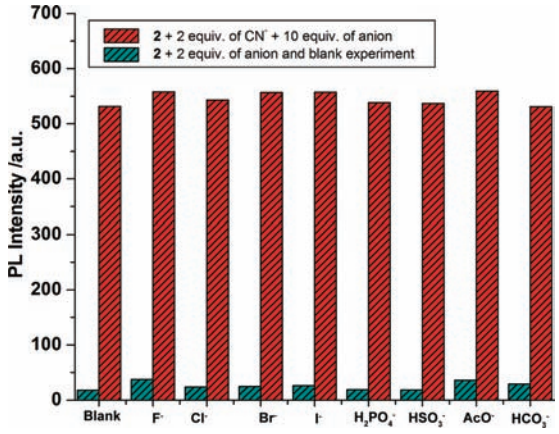

Figure 9. Behavior of $2[PF_6]_2$ toward CN^- and other anions as measured by PL in 1% aqueous acetonitrile solution.

properties. Selected calculated molecular orbital diagrams of **1**, **1**-$(CN)_2$, **2**, and **2**-$(CN)_2$ are shown in Figure 10 (and Figure S23, Supporting Information). In all compounds, the relevant occupied molecular orbitals HOMO, HOMO−1, and HOMO−2 are mainly located on the ruthenium(II) center. The two highest lying MOs, i.e., HOMO and HOMO−1, relate to the ruthenium(II) d_z orbital whereas the HOMO−2 corresponds to the ruthenium(II) t_{2g} set (see Figure S23, Supporting Information). The unoccupied molecular orbitals LUMO and LUMO+1 of complexes **1** and **2** have **PDA** (π^*) character, whereas the LUMO+2 and LUMO+3 orbitals correspond to the ancillary bipy/phen ligands. In **2**-$(CN)_2$, the LUMO and LUMO+1 are mainly located on **PDA**-$(CN)_2$ (π^*) whereas the LUMO+2 and LUMO+3 have phen (π^*) character. For **1**-$(CN)_2$, the LUMO and LUMO+1 have mixed-ligand character, i.e., **PDA**-$(CN)_2$ (π^*) and bipy (π^*), and the LUMO+2 and LUMO+3 have bipy (π^*) and **PDA**-$(CN)_2$ (π^*) character, respectively (Figure S23, Supporting Information).

To obtain insight into the electronic transitions responsible for the absorption spectra of complexes **1** and **2** and their cyanohydrin adducts, **1**-$(CN)_2$ and **2**-$(CN)_2$, time-dependent DFT (TD-DFT) calculations on optimized geometries in CH_3CN were performed. The transitions in the visible region between 370 and 600 nm are assigned to various metal-to-ligand charge-transfer bands in the singlet state (^{1}MLCT). In Table S1 (see Supporting Information) the computed vertical excitation energies and composition of the related transitions assigned to the experimental UV−vis spectra in CH_3CN are displayed. Only transitions characterized by an oscillator strength (f) larger than 0.06 are considered. With these data in hand, the experimental broad MLCT absorptions of **1** from 370 to 600 nm may be understood. The TD-DFT calculations for **1** indicate that the experimental MLCT band at ∼472 nm (2.63 eV) arises from a strong transition characterized as HOMO−1→ LUMO+1 (f = 0.3) (440 nm, 2.81 eV). Another band at 435 nm (2.85 eV) is due to the weaker transition from HOMO−2 → LUMO+2 (f = 0.12) (387 nm, 3.20 eV). In **1**-$(CN)_2$, the calculated strong transition at 418 nm (2.97 eV), which is due to the HOMO−1 → LUMO (f = 0.12) transition, is assigned to the experimental absorption band at 450 nm (2.77 eV). The other two transitions from HOMO−2 → LUMO+2 (f = 0.11) and HOMO−2 → LUMO+3 (f = 0.11) are responsible for the other absorption at 435 nm (2.85 eV). Similarly, for compound **2** the calculation shows the absorptions at 473 (2.62 eV) and 435 nm (2.85 eV) to be related to the MLCT bands from HOMO−2 → LUMO+1 (f = 0.3) (442 nm, 2.81 eV) and the HOMO−2 → LUMO +3 (f = 0.09) (386 nm, 3.21 eV), respectively. In **2**-$(CN)_2$, the experimental λ_{max} at 447 nm (2.86 eV) corresponds to a transition that relates the metal-based d orbital (HOMO−1) to the π^* of the **PDA**-$(CN)_2$ (LUMO + 1) (f = 0.07) (414 nm, 2.99 eV).

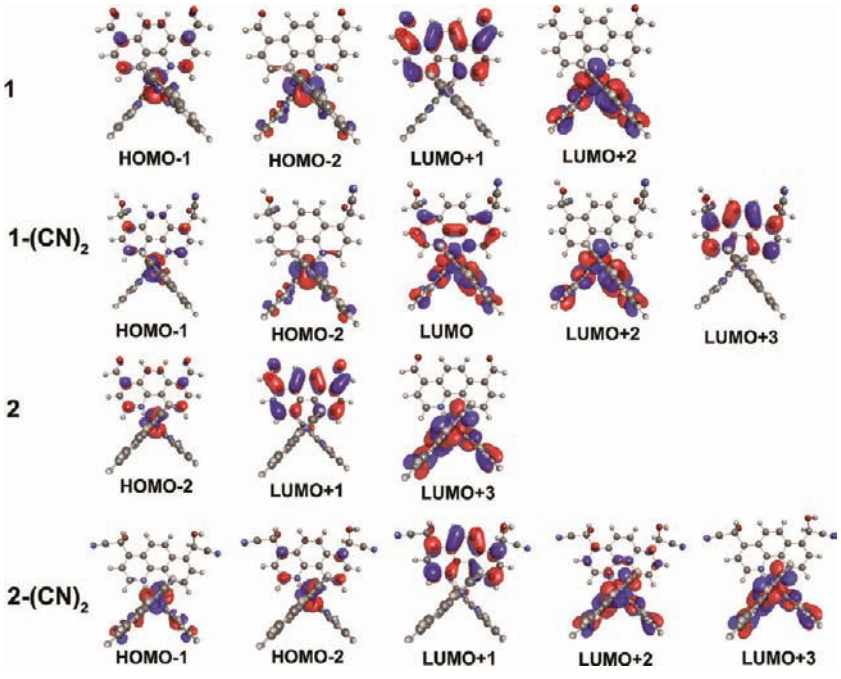

Figure 10. View of the frontier molecular orbitals (MOs) of **1**, **1**-$(CN)_2$, **2**, and **2**-$(CN)_2$ [isovalue = 0.05].

dx.doi.org/10.1021/ic2022853 | Inorg. Chem. 2012, 51, 7075−7086

Another MLCT band at 435 nm (2.85 eV) is due to combination of three major transitions, HOMO−2 → LUMO+2 (f = 0.06) (406 nm, 3.05 eV), HOMO−2 → LUMO+3 (f = 0.09) (396 nm, 3.13 eV), and HOMO−1 → LUMO+3 (f = 0.1) (400 nm, 3.09 eV), respectively. All transitions are determined to be singlet MLCT transitions (^{1}MLCT) involving the metal-based HOMO, HOMO−1, and HOMO−2 and the ligand-based LUMO, LUMO+1, LUMO+2, and LUMO+3.

CONCLUSIONS

Two new ruthenium complexes have been prepared to detect cyanide based on a cyanohydrin chemodosimeter reaction, and their mechanism of operation is carefully elucidated. Both complexes show high selectivity and sensitivity toward CN^- in pure or 1% aqueous CH_3CN using either the UV−vis or the PL channel. The immediate color change from orange-red to yellow and orange luminescence can be observed by the naked eye after CN^- addition. The high overall binding constant for **1**-$(CN)_2$ and **2**-$(CN)_2$ and immediate ∼55 fold PL intensity enhancements point to a high sensitivity of CN^- detection. The reactivity of **1**$[PF_6]_2$ and **2**$[PF_6]_2$ to CN^- is very high at room temperature, just requiring stoichiometric amounts for complete reaction within 15 s. The reactivity is higher than that of a recently reported fast CN^- probe.[27] The calculated detection limit implies that the probe can detect CN^-even at the sub-micromolar level and in the presence of many other anions. As the complex has two reacting units, a stepwise reaction is observed, which is supported by absorption, PL, and ^{1}H NMR titration. Finally, theoretical calculations furnish detailed insights into the electronic structures and transitions involved in the compounds and their cyanide adducts. The results indicate a partial MLCT switching after cyanide addition to the carbonyl groups.

EXPERIMENTAL SECTION

Materials and Physical Measurements. All chemicals were used as received from commercial suppliers (Aldrich, Alfa Aesar and Acros). ^{1}H and ^{13}C NMR spectra were measured on a Bruker Avance spectrometer using residual protic solvent as the internal standard. ESI-MS spectra were measured on a LCQ Deca Thermo Quest instrument. Infrared spectra were recorded using a Varian 1000 FT-IR instrument. Elemental analysis measurements were done using the EA 3000 CHNS. UV−vis and PL spectra were recorded on a Varian Cary 50 Bio UV−vis spectrometer and Varian Cary Eclipse fluorescence spectrometer.

Electrochemical experiments were performed using a standard three-electrode setup (Pt working electrode, Pt auxiliary electrode, silver wire as quasi-reference electrode) connected to a Princeton Applied Research model 362 potentiostat. Experiments were carried out on a 1.0 mM solution of **1**$[PF_6]_2$ or **2**$[PF_6]_2$ in dry degassed acetonitrile with 0.1 M tetra-*n*-butylammonium hexafluorophosphate (Bu_4NPF_6) as the supporting electrolyte. All potentials were measured at a scan rate of 100−200 mV s^{-1} and referenced to 1,1′-dimethylferrocene as the internal standard that has $E_{1/2}$ = −0.09 V vs $FeCp_2^{0/+}$.

DFT Calculations. All geometry optimizations were performed with the TURBOMOLE[28] program package using DFT. The B3LYP/6-31G(d) exchange correlation functional[29] was used for C, H, N, together with the LANL2DZ[30] for ruthenium. All geometries were fully optimized in the ground states (closed-shell singlet S_o). Time-dependent density functional (TD-DFT) calculations using the polarizable continuum model (PCM) nonequilibrium version,[31] in which the cavity is created by the united atom topological model as implemented in G03 for the lowest singlet−singlet and singlet−triplet excitations, were performed with a spin-restricted formalism to examine low-energy excitations at the ground-state geometry in acetonitrile at the same level of calculation as employed for geometry optimizations.

Synthesis. *Synthesis of 1,10-Phenanthroline-4,7-dicarboxaldehyde (PDA).*[22] A mixture of 4,7-dimethyl-1,10-phenanthroline (208 mg, 1.00 mmol) and selenium dioxide (448 mg, 4.00 mmol) in dioxane containing 4% H_2O (25 mL) was heated under reflux for 3 h and then filtered through Celite (2 cm bed) while kept hot. A light yellow solid separated in the cold filtrate and recrystallized from dioxane to furnish 1,10-phenanthroline-4,7-dicarboxaldehyde (**PDA**) as yellow needles. Yield: 154 mg (65%). FTIR in KBr disk (ν/cm^{-1}): 3224, 2360, 1699, 1504, 1222, 1087, 848. ESI-MS: $[C_{14}H_8N_2O_2 + H]^+$: calcd m/z, 237.07; found m/z, 237.10. ^{1}H NMR (400 MHz, $CDCl_3$): δ = 10.64 (s, 2H, 1-H, 1′-H), 9.54 (d, ^3J = 4.4, 2H, 2-H, 9-H), 9.23 (s, 2H, 5-H, 6-H), 8.10 (d, ^3J = 4.4, 2H, 3-H, 8-H). ^{13}C NMR (100 MHz, $CDCl_3$): δ = 192.4, 151.2, 146.8, 136.8, 127.2, 125.3, 124.9.

*Synthesis of [Bis(2,2′-bipyridine)(4,7-diformyl-1,10-phenanthroline)ruthenium(II) Dihexafluorophosphate] (**1**$[PF_6]_2$).* *cis*-$[Ru(bipy)_2]Cl_2{\cdot}2H_2O$[32] (0.13 g, 0.25 mmol) and 1,10-phenanthroline-4,7-dicarboxaldehyde [**PDA**] (59 mg, 0.25 mmol) were refluxed in 60 mL of degassed aqueous ethanol (ethanol/water = 2:1) at 90 °C for 14 h under N_2. An excess of NH_4PF_6 (500 mg) was added, and the mixture was stirred for another 1 h. Thereafter, the solution was concentrated under reduced pressure. The dark red-colored solid was separated from the aqueous solution by filtration, washed with distilled water, and dried under vacuum. Finally, recrystallization of the solid from acetone/chloroform provided a black red crystalline complex (154 mg, 63% yield). Diffraction-quality single crystals were obtained from an acetone, chloroform, and dichloromethane (3:2:1) mixture. Anal Calcd for $C_{34}H_{24}F_{12}N_6O_2P_2Ru{\cdot}0.3CHCl_3$ (M_w = 978.95): C, 42.08; H, 2.50; N, 8.58. Found: C, 42.34; H, 2.60; N, 8.59. FTIR in KBr (ν/cm^{-1}): 3055, 2306, 1704, 1610, 1428, 1263, 898, 840, 745. ESI-MS $[C_{34}H_{24}N_6O_2Ru]^{2+}$: calcd, m/z = 324.8; found, m/z = 324.8. ESI-MS $[C_{34}H_{24}N_6O_2RuPF_6]^+$: calcd, m/z = 794.6; found. m/z = 794.6. ^{1}H NMR (400 MHz, acetone-d_6): δ = 10.75 (s, 2H, 1-H, 1′-H), 9.46 (s, 2H, 5-H, 6-H), 8.92 (d, ^3J = 5.4 Hz, 2H, 2-H, 9-H), 8.88 (d, ^3J = 8.2 Hz, 2H, 3′-H), 8.84 (d, ^3J = 8.2 Hz, 2H, 3″-H), 8.37 (d, ^3J = 5.4 Hz, 2H, 3-H, 8-H), 8.30 (dt, ^3J = 8.0, ^4J = 1.5 Hz, 2H, 4′-H), 8.18 (dt, semicovered, ^3J = 8.0, ^4J =1.5 Hz, 2H, 4″-H), 8.17−8.15 (m, 2H, 6′-H), 7.90−7.89 (m, 2H, 6″-H), 7.67 (ddd, ^3J =7.9, ^3J =5.6 Hz, ^4J =1.2 Hz, 2H, 5′-H), 7.39 (ddd, ^3J = 7.9, ^3J =5.6 Hz, ^4J =1.2 Hz, 2H, 5″-H). ^{13}C NMR (100 MHz, acetone-d_6): δ = 193.8 (C-1, C-1′), 158.9 (4C, C-2′, C-2″), 156.5 (C-2, C-9), 154.1 (2C, C-6′), 153.8 (2C, C-6″), 150.7 (C-11, C-12), 140.6 (2C, C-4′), 140.5 (2C, C-4″), 138.2 (C-4, C-7), 131.1 (C-3, C-8), 130.0 (2C, C-5′), 129.8 (2C, C-5″), 129.2 (C-13, C-14), 128.5 (C-5, C-6), 126.5 (2C, C-3′), 126.5 (2C, C-3″).

*Synthesis of [Bis(1,10-phenanthroline)(4,7-diformyl-1,10-phenanthroline)]ruthenium(II) Dihexafluorophosphate] (**2**$[PF_6]_2$).* A mixture of *cis*-$[Ru(phen)_2]Cl_2$ (0.13 g, 0.25 mmol) and 1,10-phenanthroline-4,7-dicarboxaldehyde [**PDA**] (59 mg, 0.25 mmol) was refluxed in 60 mL of degassed aqueous ethanol (ethanol/water = 2:1) at 90 °C for 14 h under N_2. An excess of NH_4PF_6 (500 mg) was added, and the mixture was stirred for another 1 h. Then the solution was concentrated under reduced pressure. From the concentrated aqueous solution the dark red solid was filtered off, washed with distilled water, and dried under vacuum. Recrystallization from acetone/chloroform provided the black red crystalline complex (162.0 mg, 60% yield). Diffraction-quality black-colored single crystals were obtained from an acetone, chloroform, and dichloromethane (3:2:1) mixture. Anal. Calcd for $C_{38}H_{24}F_{12}N_6O_2P_2Ru{\cdot}0.77CHCl_3$ (Mw = 1079.56): C, 43.13; H, 2.31; N, 7.78, Found: C, 43.22; H, 2.03; N, 7.62. FTIR in KBr disk (ν/cm^{-1}): 3093, 1703, 1508, 1429, 1267, 957, 837, 739. ESI-MS $[C_{38}H_{24}N_6O_2Ru]^{2+}$: calcd, m/z = 348.3; found, m/z = 348.3. ESI-MS $[C_{38}H_{24}N_6O_2RuPF_6]^+$: calcd, m/z = 842.7; found, m/z = 842.1. ^{1}H NMR (400 MHz, acetone-d_6): δ(ppm) = 10.72 (s, 2H, 1-H, 1′-H); 9.47 (d, 2H, 5-H, 6-H), 8.89 (d, J = 5.4 Hz, 2H, 2-H, 9-H), 8.83 (dd, J = 8.3, 2.2 Hz, 2H, 4′-H, 4″-H), 8.83 (dd, J = 8.3, 2.2 Hz, 2H, 7′-H, 7″-H), 8.43 (dd, semicovered,

dx.doi.org/10.1021/ic2022853 | Inorg. Chem. 2012, 51, 7075−7086

J = 5.3, 1.2 Hz, 2H, 2′-H, 2″-H), 8.43 (s, 4H, 5′-H, 5″-H, 6′-H, 6″-H), 8.39 (dd, J = 5.3, 1.2 Hz, 2H, 9′-H, 9″-H), 8.25 (d, J = 5.4 Hz, 2H, 3-H, 8-H), 7.83 (dd, J = 8.3, 5.3 Hz, 2H, 3′-H, 3″-H), 7.80 (dd, J = 8.3, 5.3 Hz, 2H, 8′-H, 8″-H). ^{13}C NMR (100 MHz, acetone-d_6): δ = 193.8 (C-1, C-1′), 157.0 (C-2, C-9), 155.3 (C-2′, C-2″), 154.9 (C-9′, C-9″), 151.1 (C-11, C-12), 149.6 (C-11′, C-11″), 149.4 (C-12′, C-12″), 139.5 (C-4′, C-4″ or C-7′, C-7″), 139.4 (C-7′, C-7″ or C-4′, C-4″), 138.1(C-4, C-7), 133.1 (C-13′, C-13″, C-14′, C-14″), 131.0 (C-3, C-8), 130.2 (C-5′, C-5″), 130.2 (C-6′, C-6″), 129.1 (C-13, C-14), 128.5 (C-3′, C-3″), 128.3(C-8′, C-8″), 128.2 (C-5, C-6).

Crystallographic Studies. X-ray data of $\mathbf{1}[\mathbf{PF_6}]_2$ and $\mathbf{2}[\mathbf{PF_6}]_2$ were collected at 166 and 170 K, respectively, with a SIEMENS SMART 1K area detector diffractometer using graphite-monochromated Mo Kα radiation (λ = 0.71073 Å). An empirical absorption correction was applied using the SADABS program.[33] Structures were solved by direct methods using the program SHELXS-97[34] and refined by full matrix least-squares calculations (F^2) using the SHELXL-97[35] software. All non-H atoms were refined anisotropically against F^2 for all reflections. All hydrogen atoms were placed at their calculated positions and refined isotropically. Crystal data for $\mathbf{1}[\mathbf{PF_6}]_2$ and $\mathbf{2}[\mathbf{PF_6}]_2$ are given in Table 1. Selected bond lengths and angles are listed in Table 2. The cif files were deposited with the Cambridge Crystallographic Data Centre, and the following code was allocated: CCDC-857992 and 857993). These data can be obtained free of charge via the Internet: www.ccdc.cam.ac.uk/data_request/cif.

Table 1. Crystal Data for Compounds $\mathbf{1}[\mathbf{PF_6}]_2$ and $\mathbf{2}[\mathbf{PF_6}]_2$

	$\mathbf{1}[\mathbf{PF_6}]_2$	$\mathbf{2}[\mathbf{PF_6}]_2$
empirical formula	$C_{35}H_{25}Cl_3F_{12}N_6O_2P_2Ru$	$C_{42}H_{31}Cl_3F_{12}N_6O_3P_2Ru$
fw	1058.97	1165.09
temperature	166(2) K	170(2) K
wavelength	0.71073 Å	0.71073 Å
cryst syst	triclinic	monoclinic
space group	$P-1$	$P2_1/n$
unit cell dimens	a = 11.3135(11) Å	a = 11.5251(5) Å
	b = 12.8239(17) Å	b = 26.3548(13) Å
	c = 14.7083(17) Å	c = 16.9055(8) Å
	α = 101.288(9)°	α = 90°
	β = 93.655(10)°	β = 90.1070(10)°
	γ = 92.021(12)°	γ = 90°
vol	2085.9(4) Å^3	5134.9(4) Å^3
Z	2	4
density (calcd), Mg/m^3	1.686	1.507
F(000)	1052	2328
cryst size	0.60 × 0.60 × 0.36 mm^3	0.65 × 0.65 × 0.20 mm^3
theta range	1.93–26.75°	1.43–26.75°
reflns collected	27 281	50 012
independent reflns	8251 [R(int) = 0.0598]	10 380 [R(int) = 0.0739]
completeness to θ	26.75° (93.1%)	95.0%
abs corr	semiempirical	semiempirical
T_{max} and T_{min}	0.766 and 0.521	0.885 and 0.636
refinement method	full-matrix least-squares on F^2	full-matrix least-squares on F^2
data/restraints/parameters	8251/0/551	10 380/6/622
goodness-of-fit on F^2	1.071	1.036
final R indices [$I > 2\sigma(I)$]	$R1$ = 0.0788, $wR2$ = 0.2059	$R1$ = 0.1095, $wR2$ = 0.2929
R indices (all data)	$R1$ = 0.1071, $wR2$ = 0.2223	$R1$ = 0.1594, $wR2$ = 0.3162
largest diff. peak and hole, e·Å^{-3}	2.364 and −0.902	1.703 and −1.100

Table 2. Selected Bond Lengths [Angstroms] and Angles [degrees] for Compounds $\mathbf{1}[\mathbf{PF_6}]_2$ and $\mathbf{2}[\mathbf{PF_6}]_2$ Around the Ru(II) Center

compound $\mathbf{1}[\mathbf{PF_6}]_2$			
Ru(1)–N(2)	2.045(5)	Ru(1)–N(1)	2.051(4)
Ru(1)–N(6)	2.051(4)	Ru(1)–N(4)	2.059(5)
Ru(1)–N(3)	2.057(5)	Ru(1)–N(5)	2.058(4)
N(2)–Ru(1)–N(1)	79.31(18)	N(2)–Ru(1)–N(6)	89.06(18)
N(1)–Ru(1)–N(6)	95.88(17)	N(2)–Ru(1)–N(4)	175.84(18)
N(1)–Ru(1)–N(4)	97.78(18)	N(6)–Ru(1)–N(4)	94.22(18)
N(2)–Ru(1)–N(3)	98.38(18)	N(1)–Ru(1)–N(3)	90.84(18)
N(6)–Ru(1)–N(3)	170.80(17)	N(4)–Ru(1)–N(3)	78.60(17)
N(2)–Ru(1)–N(5)	97.14(17)	N(1)–Ru(1)–N(5)	173.73(18)
N(6)–Ru(1)–N(5)	78.81(17)	N(4)–Ru(1)–N(5)	86.02(17)
N(3)–Ru(1)–N(5)	94.81(17)		
compound $\mathbf{2}[\mathbf{PF_6}]_2$			
Ru(1)–N(1)	2.058(6)	Ru(1)–N(2)	2.043(6)
Ru(1)–N(3)	2.044(6)	Ru(1)–N(4)	2.065(6)
Ru(1)–N(5)	2.062(6)	Ru(1)–N(6)	2.070(5)
N(2)–Ru(1)–N(3)	95.6(2)	N(2)–Ru(1)–N(1)	78.8(2)
N(3)–Ru(1)–N(1)	90.6(2)	N(2)–Ru(1)–N(5)	97.3(2)
N(3)–Ru(1)–N(5)	94.8(2)	N(1)–Ru(1)–N(5)	173.6(2)
N(2)–Ru(1)–N(4)	172.9(2)	N(3)–Ru(1)–N(4)	79.9(3)
N(1)–Ru(1)–N(4)	95.6(2)	N(5)–Ru(1)–N(4)	88.7(2)
N(2)–Ru(1)–N(6)	89.4(2)	N(3)–Ru(1)–N(6)	173.2(2)
N(1)–Ru(1)–N(6)	94.8(2)	N(5)–Ru(1)–N(6)	80.0(2)
N(4)–Ru(1)–N(6)	95.5(2)		

■ ASSOCIATED CONTENT

Ⓢ Supporting Information

Crystallographic information files (CIF), all NMR data, UV–vis and PL titration data for $\mathbf{1}[\mathbf{PF_6}]_2$, CV data for $\mathbf{1}[\mathbf{PF_6}]_2$ and $\mathbf{2}[\mathbf{PF_6}]_2$. This material is available free of charge via the Internet at http://pubs.acs.org.

■ AUTHOR INFORMATION

Corresponding Author

*E-mail: schmittel@chemie.uni-siegen.de.

Notes

The authors declare no competing financial interest.

■ ACKNOWLEDGMENTS

S.K. is grateful to the Alexander von Humboldt Foundation for financial support, while additional support was provided by the DFG (Schm 647/17-1). We thank Soumen Samanta (Universität Siegen) for his help with Specfit calculations.

■ REFERENCES

(1) (a) Kulig, K. W. *Cyanide Toxicity*; U.S. Department of Health and Human Services: Atlanta, 1991. (b) Baskin, S. I.; Brewer, T. G. *Medical Aspects of Chemical and Biological Warfare*; Sidell, F., Takafuji, E. T., Franz, D. R., Eds.; TMM Publication: Washington, 1997; Chapter 10, pp 271–286.

(2) (a) Patnaik, P. *A Comprehensive Guide to the Hazardous Properties of Chemical Substance*; van Nostrand Reinhold: New York, 1992; pp 229–244. (b) Hathaway, G. J.; Proctor, N. H. *Chemical Hazards of the Workplace*, 5th ed.; John Wiley & Sons, Inc.: Hoboken, 2004; pp 190–191.

(3) (a) Beer, P. D.; Gale, P. A. *Angew. Chem., Int. Ed.* **2001**, *40*, 486–516. (b) Martínez-Máñez, R.; Sancenón, F. *Chem. Rev.* **2003**, *103*, 4419–4476. (c) Yoon, J.; Kim, S. K.; Singh, N. J.; Kim, K. S. *Chem. Soc. Rev.* **2006**, *35*, 355–360. (d) Gale, P. A. *Acc. Chem. Res.* **2006**,

39, 465−475. (e) Gunnlaugsson, T.; Glynn, M.; Tocci, G. M.; Kruger, P. E.; Pfeffer, F. M. *Coord. Chem. Rev.* **2006**, *250*, 3094−3117. (f) Lee, C.-H.; Miyaji, H.; Yoon, D.-W.; Sessler, J. L. *Chem. Commun.* **2008**, 24−34. (g) Caltagirone, C.; Gale, P. A. *Chem. Soc. Rev.* **2009**, *38*, 520−563. (h) Moragues, M. E.; Martínez-Máñez, R.; Sancenón, F. *Chem. Soc. Rev.* **2011**, *40*, 2593−2643. (i) Kim, Y.; Huh, H.-S.; Lee, M. H.; Lenov, I. L.; Zhao, H.; Gabbaï, F. P. *Chem.—Eur. J.* **2011**, *17*, 2057−2062.

(4) (a) Sun, S.-S.; Lees, A. J. *Chem. Commun.* **2000**, 1687−1688. (b) Miyaji, H.; Sessler, J. L. *Angew. Chem., Int. Ed.* **2001**, *40*, 154−157. (c) Kim, Y.-H.; Hong, J.-I. *Chem. Commun.* **2002**, 512−513. (d) Yang, Y.-K.; Tae, J. *Org. Lett.* **2006**, *8*, 5721−5723. (e) Tomasulo, M.; Sortino, S.; White, A. J. P.; Raymo, F. M. *J. Org. Chem.* **2006**, *71*, 744−753. (f) Gimeno, N.; Li, X.; Durrant, J. R.; Vilar, R. *Chem.—Eur. J.* **2008**, *14*, 3006−3012.

(5) (a) Xu, Z.; Chen, X.; Kim, H. N.; Yoon, J. *Chem. Soc. Rev.* **2010**, *39*, 127−137. (b) Jun, M. E.; Roy, B.; Ahn, K. H. *Chem. Commun.* **2011**, *47*, 7583−7601.

(6) Xu, Z.; Pan, J.; Spring, D. R.; Cui, J.; Yoon, J. *Tetrahedron* **2010**, *66*, 1678−1683.

(7) Various chemodosimeter reactions to carbonyls and its derivatives: (a) Sessler, J. L.; Cho, D.-G. *Org. Lett.* **2008**, *10*, 73−75. (b) Cho, D.-G.; Kim, J. H.; Sessler, J. L. *J. Am. Chem. Soc.* **2008**, *130*, 12163−12167. (c) Hong, S.-J.; Yoo, J.; Kim, S.-H.; Kim, J. S.; Yoon, J.; Lee, C.-H. *Chem. Commun.* **2009**, 189−191. (d) Sessler, J. L.; Cho, D.-G. *Chem. Soc. Rev.* **2009**, *38*, 1647−1662. Reaction to boron center: (e) Jin, W. J.; Fernández-Argüelles, M. T.; Costa-Fernández, J. M.; Pereiro, R.; Sanz-Medel, A. *Chem. Commun.* **2005**, 883−835. (f) Badugu, R.; Lakowicz, J. R.; Geddes, C. D. *J. Am. Chem. Soc.* **2005**, *127*, 3635−3641. (g) Ros-Lis, J. V.; Martínez-Máñez, R.; Soto, J. *Chem. Commun.* **2005**, 5260−5262. (h) Hudnall, T. W.; Gabbaï, F. P. *J. Am. Chem. Soc.* **2007**, *129*, 11978−11986. (i) Huh, J. O.; Do, Y.; Lee, M. H. *Organometallics* **2008**, *27*, 1022−1025. (j) Kim, Y.; Zhao, H.; Gabbaï, F. P. *Angew. Chem., Int. Ed.* **2009**, *48*, 4957−4960. Reaction with imine: (k) Yoshino, J.; Kano, N.; Kawashima, T. *J. Org. Chem.* **2009**, *74*, 7496−7503. Reaction with cations: (l) García, F.; García, J. M.; García-Acosta, B.; Martínez-Máñez, R.; Sancenón, F.; Soto, J. *Chem. Commun.* **2005**, 2790−2792. (m) Afkhami, A.; Sarlak, N. *Sens. Actuators, B* **2007**, *122*, 437−441. (n) Niu, H.-T.; Jiang, X.; He, J.; Cheng, J.-P. *Tetrahedron Lett.* **2009**, *50*, 6668−6671.

(8) (a) de Silva, A. P.; Gunaratne, H. Q. N.; Gunnlaugsson, T.; Huxley, A. J. M.; McCoy, C. P.; Rademacher, J. T.; Rice, T. E. *Chem. Rev.* **1997**, *97*, 1515−1566. (b) Beer, P. D.; Cadman, J. *Coord. Chem. Rev.* **2000**, *205*, 131−155. (c) Fabbrizzi, L.; Licchelli, M.; Rabaioli, G.; Taglietti, A. *Coord. Chem. Rev.* **2000**, *205*, 85−108. (d) Steed, J. W. *Chem. Soc. Rev.* **2009**, *38*, 506−519.

(9) DSSC: (a) O'Regan, B.; Grätzel, M. *Nature* **1991**, *353*, 737−740. (b) Hagfeldt, A.; Grätzel, M. *Chem. Rev.* **1995**, *95*, 49−68. (c) Nazeeruddin, M. K.; Péchy, P.; Renouard, T.; Zakeeruddin, S. M.; Humphry-Baker, R.; Comte, P.; Liska, P.; Cevey, L.; Costa, E.; Shklover, V.; Spiccia, L.; Deacon, G. B.; Bignozzi, C. A.; Grätzel, M. *J. Am. Chem. Soc.* **2001**, *123*, 1613−1624. (d) Wang, P.; Klein, C.; Humphry-Baker, R.; Zakeeruddin, S. M.; Grätzel, M. *J. Am. Chem. Soc.* **2005**, *127*, 808−809. (e) Bessho, T.; Yoneda, E.; Yum, J.-H.; Guglielmi, M.; Tavernelli, I.; Imai, H.; Rothlisberger, U.; Nazeeruddin, M. K.; Grätzel, M. *J. Am. Chem. Soc.* **2009**, *131*, 5930−5934. (f) Bomben, P. G.; Robson, K. C. D.; Sedach, P. A.; Berlinguette, C. P. *Inorg. Chem.* **2009**, *48*, 9631−9643. (g) Hagfeldt, A.; Boschloo, G.; Sun, L.; Kloo, L.; Pettersson, H. *Chem. Rev.* **2010**, *110*, 6595−6663. (h) Robson, K. C. D.; Koivisto, B. D.; Yella, A.; Sporinova, B.; Nazeeruddin, K. M.; Baumgartner, T.; Grätzel, M.; Berlinguette, C. P. *Inorg. Chem.* **2011**, *50*, 5494−5508.

(10) Photoinduced switch: (a) Badjic, J. D.; Ronconi, C. M.; Stoddart, J. F.; Balzani, V.; Silvi, S.; Credi, A. *J. Am. Chem. Soc.* **2006**, *128*, 1489−1499. (b) Petitjean, A.; Puntoriero, F.; Campagna, S.; Juris, A.; Lehn, J. M. *Eur. J. Inorg. Chem.* **2006**, *19*, 3878−3892. (c) Balzani, V.; Bergamini, G.; Marchioni, F.; Ceroni, P. *Coord. Chem. Rev.* **2006**, *250*, 1254−1266.

(11) Molecular device: (a) Ozawa, H.; Haga, M.; Sakai, K. *J. Am. Chem. Soc.* **2006**, *128*, 4926−4927. (b) Meyer, T. J. *Nature* **2008**, *451*, 778−779. (c) Liu, F.; Concepcion, J. J.; Jurss, J. W.; Cardolaccia, T.; Templeton, J. L.; Meyer, T. J. *Inorg. Chem.* **2008**, *47*, 1727−1752. (d) Fan, Y.; Zhang, L.-Y.; Dai, F.-R.; Shi, L.-X.; Chen, Z.-N. *Inorg. Chem.* **2008**, *47*, 2811−2819. (e) Zhao, S.; Arachchige, S. M.; Slebodnick, C.; Brewer, K. J. *Inorg. Chem.* **2008**, *47*, 6144−6152. (f) Shiotsuka, M.; Nishiko, N.; Keyaki, K.; Nozaki, K. *Dalton Trans.* **2010**, *39*, 1831−1835. (g) Ozawa, H.; Sakai, K. *Chem. Commun.* **2011**, *47*, 2227−2242. (h) Hirahara, M.; Masaoka, S.; Sakai, K. *Dalton Trans.* **2011**, *40*, 3967−3978.

(12) (a) Keefe, M. H.; Benkstein, K. D.; Hupp, J. T. *Coord. Chem. Rev.* **2000**, *205*, 201−228. (b) Demas, J. N.; DeGraff, B. A. *Coord. Chem. Rev.* **2001**, *211*, 317−351. (c) Wong, K. M.-C.; Yam, V. W.-W. *Coord. Chem. Rev.* **2007**, *251*, 2477−2488. (d) Zhao, Q.; Li, F.; Huang, C. *Chem. Soc. Rev.* **2010**, *39*, 3007−3030.

(13) Ruthenium complex as cation sensor: (a) Beer, P. D.; Timoshenko, V.; Maestri, M.; Passaniti, P.; Balzani, V. *Chem. Commun.* **1999**, 1755−1756. (b) Harriman, A.; Hissler, M.; Jost, P.; Wipff, G.; Ziessel, R. *J. Am. Chem. Soc.* **1999**, *121*, 14−27. (c) Wanatabe, S.; Ikishima, S.; Matsuo, T.; Yoshida, K. *J. Am. Chem. Soc.* **2001**, *123*, 8402−8403. (d) McFarland, S. A.; Finney, N. S. *Chem. Commun.* **2003**, 388−389. (e) Ajayakumar, G.; Sreenath, K.; Gopidas, K. R. *Dalton. Trans.* **2009**, 1180−1186.

(14) Ruthenium complex as anion sensor : (a) Szemes, F.; Hesek, D.; Chen, Z.; Dent, S. W.; Drew, M. G. B.; Goulden, A. J.; Graydon, A. R; Grieve, A.; Mortimer, R. J.; Wear, T.; Weightman, J. S.; Beer, P. D. *Inorg. Chem.* **1996**, *35*, 5868−5879. (b) Beer, P. D.; Szemes, F.; Balzani, V.; Salà, C. M.; Drew, M. G. B.; Dent, S. W.; Maestri, M. *J. Am. Chem. Soc.* **1997**, *119*, 11864−11875. (c) Watanabe, S.; Onogawa, O.; Komatsu, Y.; Yoshida, K. *J. Am. Chem. Soc.* **1998**, *120*, 229−230. (d) Chow, C.-F.; Lam, M. H. W.; Wong, W.-Y. *Inorg. Chem.* **2004**, *43*, 8387−8393. (e) Ghosh, A.; Ganguly, B.; Das, A. *Inorg. Chem.* **2007**, *46*, 9912−9918. (f) Cui, Y.; Mo, H.-J.; Chen, J.-C.; Niu, Y.-L.; Zhong, Y.-R.; Zheng, K.-C; Ye, B.-H. *Inorg. Chem.* **2007**, *46*, 6427−6436. (g) Cui, Y.; Niu, Y.-L.; Cao, M.-L.; Wang, K.; Mo, H.-J.; Zhong, Y.-R.; Ye, B.-H. *Inorg. Chem.* **2008**, *47*, 5616−5624. (h) Zapata, F.; Caballero, A.; Espinosa, A.; Tárraga, A.; Molina, P. *J. Org. Chem.* **2008**, *73*, 4034−4044. (i) Berni, E.; Gosse, I.; Badocco, D.; Pastore, P.; Sojic, N.; Pinet, S. *Chem.—Eur. J.* **2009**, *15*, 5145−5152.

(15) Oxygen sensor: (a) Carraway, E. R.; Demas, J. N.; DeGraff, B. A.; Bacon, J. R. *Anal. Chem.* **1991**, *63*, 337−342. (b) Rosenzweig, Z.; Kopelman, R. *Anal. Chem.* **1995**, *67*, 2650−2654. (c) Zhao, Y.; Richman, A.; Storey, C.; Radford, N. B.; Pantano, P. *Anal. Chem.* **1999**, *71*, 3887−3893. (d) Dobrucki, J. W. *J. Photochem. Photobiol., B* **2001**, *65*, 136−144. (e) McGee, K. A.; Veltkamp, D. J.; Marquardt, B. J.; Mann, K. R. *J. Am. Chem. Soc.* **2007**, *129*, 15092−15093. (f) McGee, K. A.; Marquardt, B. J.; Mann, K. R. *Inorg. Chem.* **2008**, *47*, 9143−9145. (g) McGee, K. A.; Mann, K. R. *J. Am. Chem. Soc.* **2009**, *131*, 1896−1902. (h) Payne, S. J.; Fiore, G. L.; Fraser, C. L.; Demas, J. N. *Anal. Chem.* **2010**, *82*, 917−921. (i) Ji, S.; Wu, W.; Wu, W.; Song, P.; Han, K.; Wang, Z.; Liu, S.; Guo, H.; Zhao, J. *J. Mater. Chem.* **2010**, *20*, 1953−1963.

(16) DNA sensor/probe: (a) Ruba, E.; Hart, J. R.; Barton, J. K. *Inorg. Chem.* **2004**, *43*, 4570−4578. (b) Foxon, S. P.; Metcalfe, C.; Adams, H.; Webb, M.; Thomas, J. A. *Inorg. Chem.* **2007**, *46*, 409−416. (c) Zhang, J.; Qi, H.; Li, Y.; Yang, J.; Gao, Q.; Zhang, C. *Anal. Chem.* **2008**, *80*, 2888−2894. IP3 sensor: (d) Aoki, S.; Zulkefeli, M.; Shiro, M.; Kohsako, M.; Takeda, K.; Kimura, E. *J. Am. Chem. Soc.* **2005**, *127*, 9129−9139. Cysteine probe: (e) Zhang, R.; Yu, X.; Ye, Z.; Wang, G.; Zhang, W.; Yuan, J. *Inorg. Chem.* **2010**, *49*, 7898−7903. Thiol probe: (f) Ji, S. M.; Guo, H. M.; Yuan, X. L.; Li, X. H.; Ding, H. D.; Gao, P.; Zhao, C. X.; Wu, W. T.; Wu, W. H.; Zhao, J. Z. *Org. Lett.* **2010**, *12*, 2876−2879. NO probe: (g) Zhang, R.; Ye, Z.; Wang, G.; Zhang, W.; Yuan, J. *Chem.—Eur. J.* **2010**, *16*, 6884−6891.

(17) (a) Wade, C. R.; Gabbaï, F. P. *Inorg. Chem.* **2010**, *49*, 714−720. (b) Sun, Y.; Hudson, Z. M.; Rao, Y.; Wang, S. *Inorg. Chem.* **2011**, *50*, 3373−3378.

(18) (a) Kim, Y. K.; Lee, Y.-H.; Lee, H.-Y.; Kim, M. K.; Cha, G. S.; Ahn, K. H. *Org. Lett.* **2003**, *5*, 4003−4006. (b) Lee, K.-S.; Kim, H.-J.; Kim, G.-H.; Shin, I.; Hong, J.-I. *Org. Lett.* **2008**, *10*, 49−51.

(c) Kim, D.-S.; Chung, Y.-M.; Jun, M.; Ahn, K. H. *J. Org. Chem.* **2009**, *74*, 4849−4854.
(19) (a) Chung, Y.; Lee, H.; Ahn, K. H. *J. Org. Chem.* **2006**, *71*, 9470−9474. (b) Ekmekci, Z.; Yilmaz, M. D.; Akkaya, E. U. *Org. Lett.* **2008**, *10*, 461−464. (c) Lee, H.; Chung, Y. M.; Ahn, K. H. *Tetrahedron Lett.* **2008**, *49*, 5544−5547. (d) Miyaji, H.; Kim, D.-S.; Chang, B.-Y.; Park, E.; Park, S.-M.; Ahn, K. H. *Chem. Commun.* **2008**, 753−755. (e) Niu, H.-T.; Su, D.; Jiang, X.; Yang, W.; Yin, Z.; He, J.; Cheng, J.-P. *Org. Biomol. Chem.* **2008**, *6*, 3038−3040.
(20) (a) Anzenbacher, P. Jr.; Tyson, D.; Jursíková, K.; Castellano, F. *J. Am. Chem. Soc.* **2002**, *124*, 6232−6233. (b) Mizuno, T.; Wei, W.-H.; Eller, L. R.; Sessler, J. L. *J. Am. Chem. Soc.* **2002**, *124*, 1134−1135. (c) Lou, B.; Chen, Z.-Q.; Bian, Z.-Q.; Huang, C.-H. *New J. Chem.* **2010**, *34*, 132−136. (d) Saha, D.; Das, S.; Bhaumik, C.; Dutta, S.; Baitalik, S. *Inorg. Chem.* **2010**, *49*, 2334−2348.
(21) (a) Schmittel, M.; Lin, H.-W.; Thiel, E.; Meixner, A. J.; Ammon, H. *Dalton Trans.* **2006**, 4020−4028. (b) Schmittel, M.; Lin, H. *Angew. Chem., Int. Ed.* **2007**, *46*, 893−896. (c) Schmittel, M.; Lin, H. *Inorg. Chem.* **2007**, *46*, 9139−9145. (d) Lin, H.; Cinar, M. E.; Schmittel, M. *Dalton Trans.* **2010**, *39*, 5130−5138.
(22) Higashi, T.; Inami, K.; Mochizuki, M. *J. Heterocycl. Chem.* **2008**, *45*, 1889−1892.
(23) (a) Tokel-Takvoryan, N. E.; Hemingway, R. E.; Bard, A. J. *J. Am. Chem. Soc.* **1973**, *95*, 6582. (b) Ji, Z.; Huang, S. D.; Guadalupe, A. R. *Inorg. Chim. Acta* **2000**, *305*, 127.
(24) (a) Pyo, S.; Pérez-Cordero, E.; Bott, S. G.; Echegoyen, L. *Inorg. Chem.* **1999**, *38*, 3337−3343. (b) Baitalik, S.; Flörke, U.; Nag, K. *Inorg. Chem.* **1999**, *38*, 3296−3308. (c) Derossi, S.; Adams, H.; Ward, M. D. *Dalton Trans.* **2007**, 33−36. (d) Bhaumik, C.; Das, S.; Saha, D.; Dutta, S.; Baitalik, S. *Inorg. Chem.* **2010**, *49*, 5049−5062. (e) Das, S.; Saha, D.; Bhaumik, C.; Dutta, S.; Baitalik, S. *Dalton Trans.* **2010**, *39*, 4162−4169. (f) Saha, D.; Das, S.; Maity, D.; Dutta, S.; Baitalik, S. *Inorg. Chem.* **2011**, *50*, 46−61.
(25) *SPECFIT, Global Analysis system*, Version 3.0.32. Gampp, H.; Maeder, M.; Meyer, C. J.; Zuberbühler, A. D. *Talanta* **1985**, *32*, 257−264.
(26) Chen, C.-L.; Chen, Y.-H.; Chen, C.-Y.; Sun, S.-S. *Org. Lett.* **2006**, *8*, 5053−5056.
(27) Yuan, L.; Lin, W.; Yang, Y.; Song, J.; Wang, J. *Org. Lett.* **2011**, *13*, 3730−3733.
(28) *Turbomole*, version 5.9; Turbomole GmbH, http://www.turbomole.com. Ahlrichs, R.; Bär, M.; Häser, M.; Horn, H.; Kölmel, C. *Chem. Phys. Lett.* **1989**, *162*, 165−169.
(29) Becke, A. D. *J. Chem. Phys.* **1993**, *98*, 5648−5652.
(30) Hay, P. J.; Wadt, W. R. *J. Chem. Phys.* **1985**, *82*, 299−310.
(31) Cossi, M.; Barone, V. *J. Chem. Phys.* **2001**, *115*, 4708−4717.
(32) Sullivan, B. P.; Salmon, D. J.; Meyer, T. J. *Inorg. Chem.* **1978**, *17*, 3334−3341.
(33) *SADABS, Area Detector Absorption Correction Program*; Bruker Analytical X-ray: Madison WI, 1997.
(34) Sheldrick, G. M. *Acta Crystallogr., Sect. A* **1990**, *46*, 467−473.
(35) (a) Sheldrick, G. M. *SHELXL-97: Program for Crystal Structure Solution and Refinements*; Universität Göttingen: Göttingen, Germany, 1999. (b) Sheldrick, G. M. *Acta Crystallogr., Sect. A* **2008**, *64*, 112−122.